**EPJ manuscript No.**
(will be inserted by the editor)

# Dynamic Versus Quasi-static Loading of X65 Offshore Steel Pipes

Martin Kristoffersen[a], Tore Børvik, Magnus Langseth, and Odd Sture Hopperstad

Structural Impact Laboratory, Centre for Research-Based Innovation (CRI), Department of Structural Engineering, Norwegian University of Science and Technology, Rich. Birkelands vei 1A, NO-7491 Trondheim, Norway

**Abstract.** Anchors or trawl gear occasionally impact offshore pipelines, resulting in large local and global deformations. Impact velocities are typically less than 5 m/s, but local strain rates may be very high. In this study strain rate effects in an X65 offshore material was characterised by split Hopkinson bar tests, while the cross-section homogeneity and possible anisotropic behaviour were determined by quasi-static material tests. Further, dynamic impact tests at prescribed velocities were carried out on simply supported full scale X65 steel pipes. Next, deformation-controlled quasi-static tests with the same boundary conditions were conducted. The level of deformation in the quasi-static tests were set to be equal to what was attained in the dynamic tests. Finally, an assessment of the differences between the dynamically and quasi-statically loaded pipes was made in terms of force-displacement response, energy absorbed, and fracture. An optical light microscope and a scanning electron microscope were used to investigate fracture surfaces arising from the various tests.

## 1 Introduction

Transportation of oil and gas by means of pipelines is a crucial part of the offshore industry [1]. Impacts from trawl gear and anchors can severely damage pipelines (see e.g. Ref. [2]), occasionally without obvious visual cues. This necesstates an assessment regarding the hazards and potential damage following such an event [3], as failure in a pipeline transporting oil and/or gas could result in severe environmental damage and economic losses. After the initial impact, the object may entangle with the pipeline and drag it out of position before it is finally released and thereby rebounds towards its initial position [4]. The Petroleum Safety Authority of Norway has published a comprehensive list online of accidental damage to structures in the North Sea and Norwegian Sea [5]. Det Norske Veritas (DNV) has published a recommended practice for handling interference between pipelines and trawl gear [6].

The open literature provides several studies on pipeline impact. Manes et al. [7] attempted to recreate the loading sequence of impact, hooking, pull-over and subsequent release by subjecting plate strips taken from a longitudinally welded X65 offshore pipeline to quasi-static three point bending tests. The strips were then pulled

[a] e-mail: martin.kristoffersen@ntnu.no

straight and checked for cracks, which was observed in only one specimen. Full-scale tests with dynamic impact and quasi-static stretching has also been carried out [8], where the stretch part always produced cracks.

This study presents dynamic impact loading and quasi-static three-point bending of a seamless, simply supported pipe made from X65 steel. The material is commonly used in offshore pipelines transporting oil and/or gas [9]. A material test programme was performed on specimens taken in different directions and from different locations across the pipe's cross-section. Dynamic material tests were also conducted. For the component tests, a pendulum accelerator [10] was used to launch a trolley with a given mass and velocity against the pipe, whereas the quasi-static tests were performed in an Instron 1332 testing rig. Finally, the test components were examined for fracture and a comparison between dynamic and quasi-static loading was carried out. Cracks discovered in the dynamic component tests were examined closely by microscopy.

## 2 Material tests

Uniaxial tension tests on smooth axisymmetric specimens have been conducted. The geometry of the specimens used in all material tests herein is shown in Fig. 1, where all measures are in mm. Specimens were taken from different positions (labelled north, south, east and west) across the cross-section to check the homogeneity, and from different directions with respect to the pipe's longitudinal axis (0°, 45° and 90°).

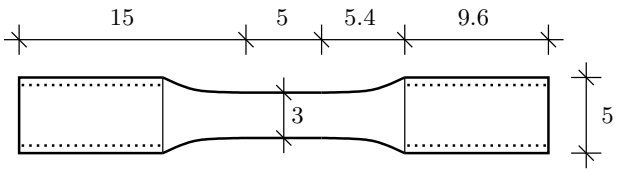


**Fig. 1.** Geometry of specimens used in quasi-static and dynamic uniaxial tensile tests.

During testing, the force, the cross-head displacement and the specimen's diameter reduction were measured continuously. Measurement of the diameter at minimum cross-section of the specimen was made possible using an in-house measuring rig with two perpendicular lasers that accurately measure the specimen diameter until fracture (see Ref. [11] for a detailed description of the setup).

By using diameter reduction measurements it is possible to calculate the true (Cauchy) stress $\sigma$ and the true (logarithmic) strain $\varepsilon$ through the well known formulas

$$\sigma = \frac{P}{A} \qquad\qquad \varepsilon = \ln\left(\frac{A_0}{A}\right) \tag{1}$$

where $P$ is the force measured by the load cell on the Zwick machine and $A_0$ is the specimen's initial cross-sectional area calculated by $A_0 = (\pi/4)\, D_0^2$, $D_0$ being the initial diameter. $A$ is the current area of the cross-section, obtained by $A = (\pi/4)\, D_1 D_2$, in which $D_1$ and $D_2$ are the diameters measured by the two lasers. Assuming additive decomposition of the elastic and plastic strains, the plastic strain $\varepsilon^p$ can be found through the relation

$$\varepsilon^p = \varepsilon - \sigma/E \tag{2}$$

where $E = 208\,000$ MPa is Young's modulus. It should be noted that plastic incompressibility and negligible elastic strains are assumed in Eq. (1), and that after

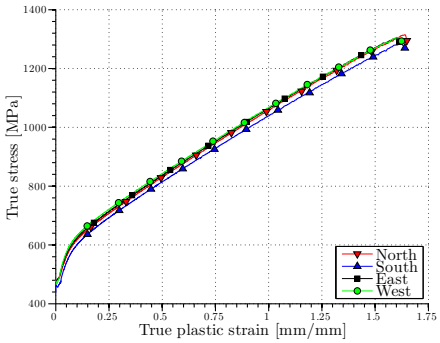


(a) Section homogeneity

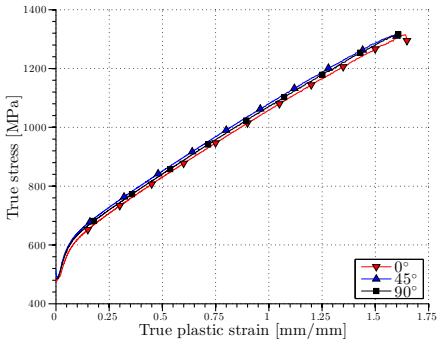


(b) Anisotropy

**Fig. 2.** True stress-true plastic strain curves from quasi-static (strain rate 0.001 $s^{-1}$) tensile tests regarding cross-section homogeneity and anisotropy [8].

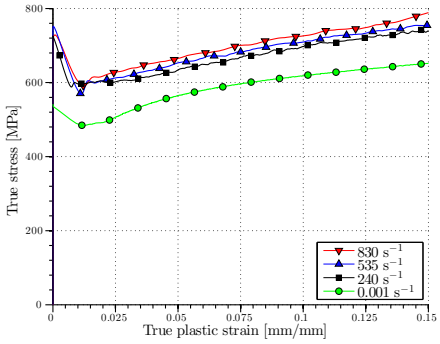


(a) True stress vs. true plastic strain

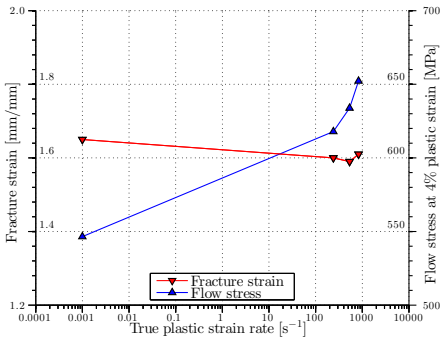


(b) Fracture strain and flow stress vs. plastic strain rate

**Fig. 3.** Data from dynamic tensile tests on uniaxial specimens [12].

necking the measured true stress $\sigma$ and true strain $\varepsilon$ represent average values over the minimum cross-section.

Results from the section homogeneity tests are presented in Fig. 2(a), plotted as true stress vs. true strain, while part (b) shows the anisotropy results. The material used here has (based on average values from 12 tests) a yield stress $\sigma_0$ of 478±15 MPa and an ultimate tensile strength $\sigma_u$ of 572±14 MPa, at which point the engineering strain $e\,(\sigma_u)$ reaches 0.143±0.010. It further strain hardens to a maximum true stress $\sigma_f$ of 1314±12 MPa and has a true failure strain $\varepsilon_f = 1.613 \pm 0.029$. All specimens failed by a ductile cup-and-cone fracture, and they remained circular throughout the test. Two tests at three different true strain rates $\dot{\varepsilon}_0$ were carried out in a split Hopkinson tension bar (SHTB); 240 $s^{-1}$, 535 $s^{-1}$ and 830 $s^{-1}$. A description of how the test rig works can be found in Ref. [13]. Fig. 3(a) shows that the flow stress increases with increasing strain rate, whereas the fracture strain remains of the same order, as seen in Fig. 3(b). The fracture strain $\varepsilon_f$ was calculated using Eq. (3), which is obtained from Eq. (1) by inserting the initial diameter $D_0$ and the diameter at fracture $D_f$ (measured by a micrometer screw) when calculating $A_0$ and $A$,

$$\varepsilon_f = 2\ln\left(\frac{D_0}{D_f}\right) \tag{3}$$

under the assumption of isotropic behaviour (i.e. the fracture surface is circular).

In summary, it can be said that the material presents itself as homogeneous and isotropic, and with an increase in flow stress for increasing strain rates (about 20% increase for the highest strain rate). The fracture strain appeared unaffected by the strain rate, with an average value of $1.598 \pm 0.029$.

## 3 Component tests

### 3.1 Setup

Pipes were delivered with a nominal inner diameter $D_i = 123$ mm and pipe wall thickness $T = 9.5$ mm. The middle section was lathed down to approximately $t = 4$ mm to obtain a diameter to thickness ratio of about 30, which is common in many offshore pipelines [14]. This does, however, result in a slightly uneven thickness and a slightly varying thickness between the pipes. A span of 1000 mm was used, with the pipe being simply supported. The supports were massive steel cylinders with diameter 50 mm, while the indenter chosen was the sharpest in the DNV guidelines [6], i.e. a nose made of massive steel with 10 mm radius. This nose was used for both the dynamic and quasi-static tests. A sketch of the general setup can be viewed in Fig. 4.

As mentioned, the loading is applied either dynamically or quasi-statically. In the dynamic case, the nose is mounted to a trolley with mass $m = 1472$ kg travelling on rails, and with a prescribed initial velocity which determines the kinetic energy to be absorbed. Two different initial velocities $v_0$ were considered, 3.2 m/s and 5.1 m/s, which is in line with what is laid out in the DNV guidelines [6]. For the two quasi-static tests the loading was applied through a deformation-controlled Instron 1332 universal testing machine and subsequently unloaded, with a deformation rate of 10 mm/min. The level of deformation was determined by the preceding dynamic tests – the same deformation was attempted applied quasi-statically as obtained in the two dynamic cases. It is a bit difficult to obtain the exact same permanent deformation in practice as the magnitude of the elastic deformation is unknown and only estimated. Unfortunately the software accompanying the test rig stops logging data when unloading commences, making the quantity of elastic deformation still somewhat intangible.

In total four pipes were tested, two dynamically (D1 and D2) and two quasi-statically (Q1 and Q2). The resulting deformation from D1 was then applied to Q1, and equivalently for D2 and Q2. See Table 1 and Fig. 5 for details.

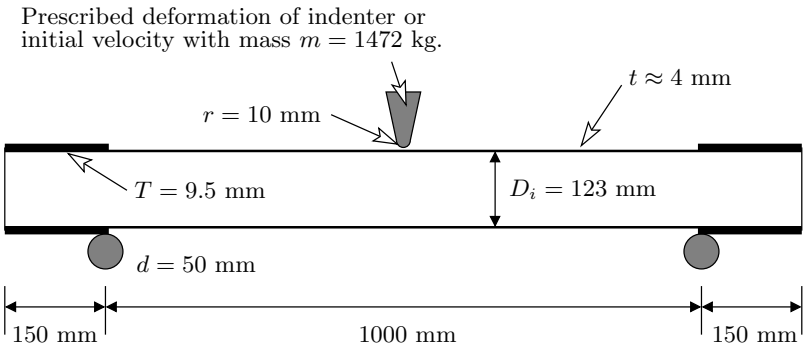


**Fig. 4.** Sketch of setup used in dynamic and quasi-static component tests.

**Table 1.** Experimental matrix for component tests for fracture investigation. See Fig. 5 for explanation of measurements.

| **Pipe** | | **D1** | **D2** | **Q1** | **Q2** |
|---|---|---|---|---|---|
| Trolley mass | [kg] | 1472 | 1472 | - | - |
| Nose radius | [mm] | 10 | 10 | 10 | 10 |
| Avg. thickness | [mm] | 3.89 ±0.36 | 3.86 ±0.34 | 3.90 ±0.26 | 3.74 ±0.25 |
| | | *Test results* | | | |
| Initial velocity | [m/s] | 3.24 | 5.13 | - | - |
| Def. rate | $[\frac{\text{mm}}{\text{min}}]$ | - | - | 10 | 10 |
| Kin. energy | [J] | 7708 | 19356 | - | - |
| Abs. energy* | [J] | 7642 | 11736 | 6975 | 10374 |
| Peak force | [kN] | 70.7 | 72.7 | 60.6 | 55.5 |
| $w_i$ | [mm] | 170 | 333 | 161 | 380 |
| $L_{\text{N-N}}$ | [mm] | 1250 | 1104 | 1249 | 1042 |
| $d_{\text{N-S}}$ | [mm] | 60 | 22 | 64 | 26 |
| $d_{\text{E-W}}$ | [mm] | 180 | 199 | 178 | 202 |
| $\alpha$ | [deg] | 12 | 30 | 12 | 31 |

*Estimated by integrating the measured force-displacement curve to max. common displacement.

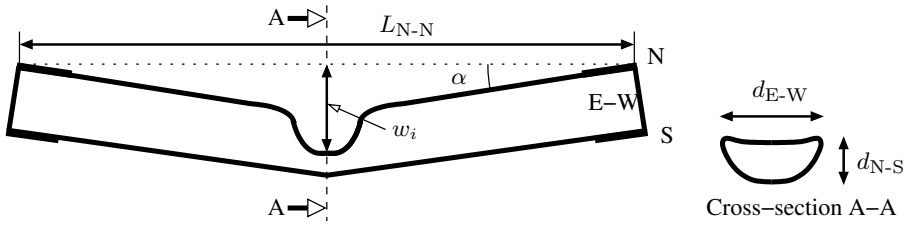


**Fig. 5.** Typical outline of deformation shape (not to scale) of pipes after load at midspan, along with explanation of measurements given in Table 1.

### 3.2 Results

Force-displacement curves for all four pipes are plotted in Fig. 6, with some oscillations in the dynamic ones. As the impact tests take place over a small span of time, contact conditions close to the load cell as well as stress waves and their possible reflections may influence the recorded force-displacement curves, as is evident here. From twelve prior dynamic impact tests (including D1 and D2) in the range 2.7 m/s to 5.2 m/s it was concluded that the initial velocity was of minor importance with respect to the peak force, and that the thickness and local contact conditions were more important [8,12].

The peak force in the two dynamic impact tests presented here (D1 and D2) averaged at 71.7 kN, whereas the quasi-static counterparts (Q1 and Q2) averaged at 58.1 kN, meaning that the peak force is reduced by roughly 20% when going from dynamic to quasi-static loading. This is in accordance with expectations, as inertia forces and strain rate effects (see Fig. 3) announce their presence. In effect, this means that for a given deformation more energy is absorbed if the event is dynamic. The two quasi-static tests are for all practical purposes identical, except for the prescribed deformation. Hence the difference in peak force is mainly attributed to the difference in thickness (see Table 1), which is the only notable difference in initial conditions between Q1 and Q2. Q1 reached a very similar deformation compared with D1. For

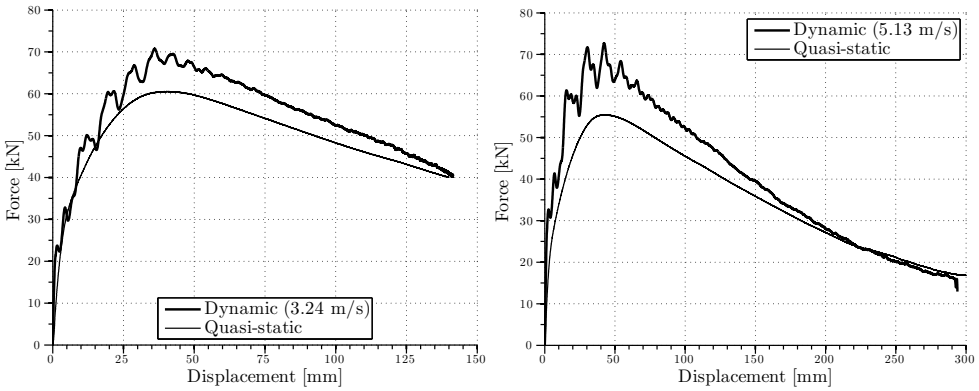


(a) Series 1 (b) Series 2

**Fig. 6.** Results from the dynamic impact tests and the quasi-static bending tests. Note the difference in scale between the ascissa on the two figures.

the Q2 test, the deformation applied was slightly too large. When determining the energy absorbed in Table 1, the curve is integrated up to the point of maximum common deformation. The energy absorbed by quasi-static deformation (to the same deformation level) is then estimated to about 90% of the dynamically absorbed one. It should be mentioned that when testing pipe D2, the trolley hit the buffer in the rig as the pipe was severely deformed (see Ref. [8]).

Some fraction of the initial kinetic energy in the dynamic tests necessarily contributes to accelerating the pipe, thereby increasing the force level registered by the load cell. Part of the energy will also be dissipated through friction and heat in the trolley and the rails. This is, however, assumed to be of minor importance. As mentioned, strain rate effects in the material also contribute to increasing the force level as indicated by the SHTB test results in Fig. 3.

A typical outline of a deformed pipe is sketched in Fig. 5. Note that the quantity $w_i$ is measured post-deformation, meaning that the rotation of the end sections contributes to the value and this will therefore differ from what was registered during testing. As indicated, the dynamic tests were performed first, and pipe D2 presented itself with a clearly visible crack in the dented area (see Fig. 7). For pipe D1 no such cracks were visible on the surface. It was therefore of great interest to check whether a pipe deformed quasi-statically to the same level (and even beyond) would suffer the

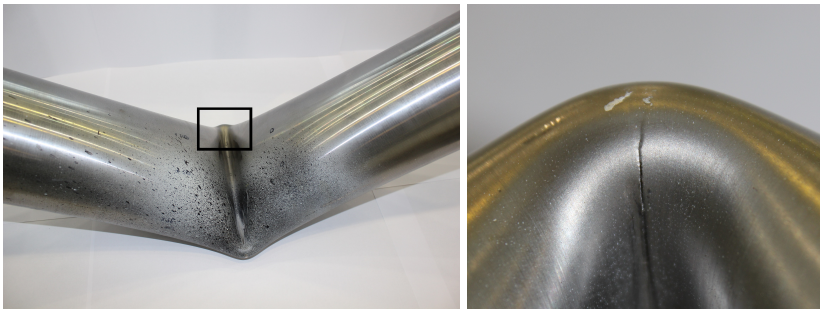

(a) Dent in pipe D2 (b) Crack in pipe D2

**Fig. 7.** Dynamic impact against pipe D2 caused a clearly visible crack.

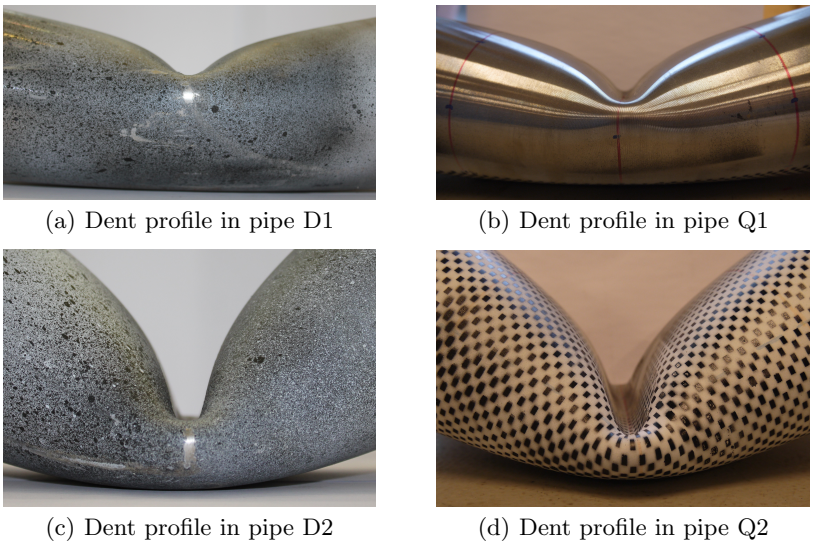

(a) Dent profile in pipe D1

(b) Dent profile in pipe Q1

(c) Dent profile in pipe D2

(d) Dent profile in pipe Q2

**Fig. 8.** Comparison of dents after dynamic deformation (left column) and static deformation (right column).

same cracking. Despite very similar deformation, no cracks were visible on the surface of the quasi-statically deformed pipe Q2 (or for Q1). This is a very clear indication that the problem being dynamic is a crucial factor.

The magnitude of deformation between pipes D1 and Q1 was indeed very similar, as Figs. 8(a) and (b) can confirm (applicable to pipes D2 and Q2 in (c) and (d) as well). Local deformation in terms of $d_{\text{N-S}}$ and $d_{\text{E-W}}$ is also quite similar (measuremensts in Table 1). The dynamically deformed pipes seem to have a slightly larger curvature locally, but this is difficult to quantify.

The springback/rebound occuring directly after maximum deformation in the dynamic tests is a likely candidate to initiate the observed fracture. On the side of the pipe's dent facing the indenter, the material suffers great compression during the course of deformation. In the dynamic tests, this compression is reversed into tension within a few milliseconds. This is thought to be the event to initiate the cracks. When doing this quasi-statically, this load reversal is slow and no rapid change of loading direction takes place, thereby gently unloading the pipe and hence reducing the likelyhood of fracture.

Doing quasi-static tests to replace dynamic tests may therefore be a directly dangerous way of conducting experiments. Also, obtaining an "equivalent static load" as a replacement for a dynamic load as suggested in NS-EN 1991-1-7 [15] is not necessarily "equivalent" at all. So in order to obtain a meaningful equivalent static load, it must elicit the same response in the structure – which in this case appears to be very unlikely.

## 4 Fracture investigations

Fracture surfaces from the material tests presented in Fig. 2 were investigated, and they showed a classic ductile character with void nucleation, growth and coalescence completely in accordance with expectations and as shown in Fig. 9. With a logarithmic fracture strain of about 1.6 the material is quite ductile. This type of fracture has been studied extensively in the literature (see e.g. Refs. [16–18]).

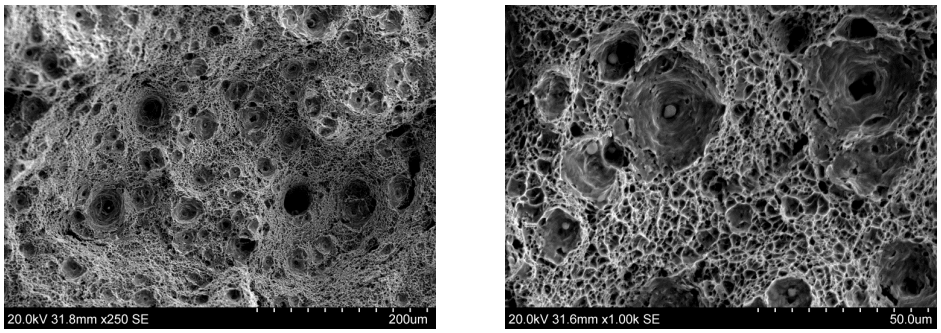


(a) Zoom ×250 (b) Zoom ×1000

**Fig. 9.** Ductile fracture surfaces from material tests.

Next, the crack in pipe D2 was examined. Fig. 10(a) displays a sample cut from this pipe, with the vertical arrow indicating the impact direction and the horizontal arrow highlighting the macroscopically visible crack. The fracture surface arising here was of a completely different character compared with the fracture from the material tests – Fig. 10(b) looks like a textbook example of a cleavage fracture, typically associated with brittle materials or low temperatures [19]. This shows that a cleavage fracture may be preceded by large scale plasticity, as also noted by Smith [20]. Almost any phenomena contributing to an increase in yield stress, such as high strain rates, constrained plastic flow, a triaxial stress state, and low temperature can increase the susceptibility to cleavage fracture [21].

Pipe D1 showed no immediate tendency to crack initiation, neither by visual inspection nor in the optical microscope. The surface was intact and no internal cracks were seen. Closer investigation in the optical light microscope of sample 2, depicted in Fig. 11(a) with the arrow indicating the impact direction, revealed a latent crack approximately 300 $\mu$m long in the middle of the material thickness (see Fig. 11(b)). The crack was found around the grain and phase boundaries, and can be very hard to detect. Samples were also cut from pipes Q1 and Q2 and checked for fracture with both the naked eye and in the microscope. No fracture was found unlike in the dynamic tests, although a heavily deformed microstructure was observed (see Fig. 12). Grains were elongated perpendicularly to the compression direction, thereby creating aligned grain boundaries which could serve as fracture planes which in turn

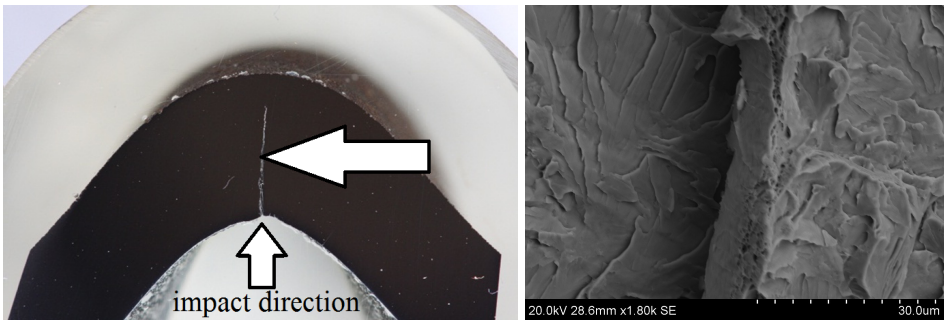


(a) Macroscopically visible crack in pipe D2 [8] (b) Fracture surface in pipe D2, ×1800

**Fig. 10.** Pipe D2 had a clearly visible crack through 75% of the pipe wall thickness after impact at 5.1 m/s.

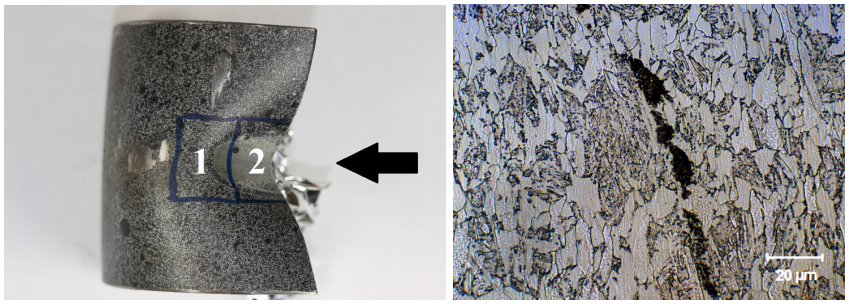


(a) Overview of samples 1 and 2 from D1 (b) Crack from sample 2, ×100

**Fig. 11.** Investigation for fracture of pipe D1 impacted at 3.2 m/s.

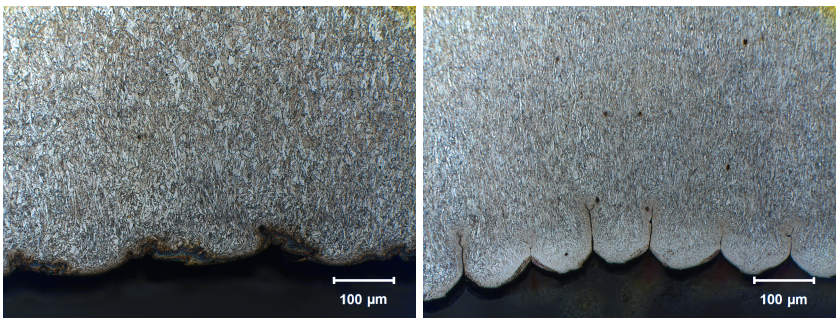


(a) Pipe Q1 ×20 (b) Pipe Q2 ×20

**Fig. 12.** Compressive side of pipe wall in the dent caused by quasi-static deformation.

may, after a rapid load reversal during springback, emerge as cleavage fracture. Based on these observations, the problem being dynamic is deemed a crucial factor. In the compressed zone of the dent some tendencies to crack initiation was observed in pipe Q2 due to the lathing grooves on the pipe surface as seen in Fig. 12(b), where the microstructure is heavily compressed.

## 5 Discussion and conclusions

The quasi-static uniaxial tensile tests from different positions across the cross-section and from different directions (see Fig. 2) revealed clear indications of a homogeneous and isotropic material. Circular fracture surfaces and the perpendicularly measured diameter reduction during testing confirmed this assertion. Increasing strain rates led to an increased flow stress. At 4% plastic strain and a strain rate of about 830 $s^{-1}$, the flow stress was 20% higher compared with the quasi-static case as shown in Fig. 3.

When going from dynamic to quasi-static loading in the component tests the force level drops with about 20%, meaning that for a given deformation more energy is absorbed if the event is dynamic. When the deformation attains its maximum value in the dynamic tests, the dynamic force is very close to the static value (see Fig. 6).

An examination of the pipes tested quasi-statically, Q1 and Q2, revealed that no fracture was visible to the naked eye or in the microscope, as opposed to D1 and D2 which both had initiated fracture. This supports the hypothesis that fracture initiates during the rapid springback after maximum deformation is attained in the dynamic tests. The fracture surface in D2 was clearly a cleavage type fracture, provoked by

high compressive strains and restrained plastic flow, before a swift reversal into tension. During compression microcracks will initiate and extend perpendicularly to the load direction [22], thereby causing earlier coalescence during subsequent tension. By loading diabolo-shaped specimen quasi-statically in a compression-tension sequence, cleavage fracture surfaces have been reproduced in this material [8]. Cracked particles were also observed due to this loading, which may cause stress concentrations and increase the likelyhood of fracture.

The work has been carried out with financial support from the Research Council of Norway and SIMLab Centre for Research-based Innovation (CRI) at the Norwegian University of Science and Technology.

## References

1. N. Jones, Journal of Strain Analysis for Engineering Design **45**, 451 (2010)
2. Statoil ASA, *Small gas leak from Kvitebjørn pipeline* (Cited 27.10.2014), `http://www.statoil.com/en/NewsAndMedia/News/2008/Pages/gasleakkvitebjorn.aspx`
3. N. Jones, R. Birch, International Journal of Pressure Vessel Technology **118**, 464 (1996)
4. M. Kristoffersen, T. Børvik, M. Langseth, H. Ilstad, E. Levold, O. Hopperstad, Proceedings of the ASME 2013 32nd International Conference on Ocean, Offshore and Arctic Engineering (2013)
5. Petroleumstilsynet, *Damage and incidents involving load-bearing structures and pipeline systems*, Petroleum Safety Authority Norway (Cited 27.10.2014), `http://www.ptil.no/news/damage-and-incidents-involving-load-bearing-structures-and-pipeline-systems-article4306-79.html?lang=en\_US`
6. DNV, *Offshore standard DNV-RP-F111: Interference between trawl gear and pipelines*, Det Norske Veritas (2010)
7. A. Manes, R. Porcaro, H. Ilstad, E. Levold, M. Langseth, T. Børvik, Ships and Offshore Structures **7**, 371 (2012)
8. M. Kristoffersen, T. Børvik, I. Westermann, M. Langseth, O. Hopperstad, International Journal of Solids and Structures **50**, 3430 (2013)
9. C.K. Oh, Y.J. Kim, J.H. Baek, W.S. Kim, International Journal of Fracture **143**, 119 (2007)
10. A. Hanssen, T. Auestad, T. Tryland, M. Langseth, International Journal of Crashworthiness **8**, 385 (2003)
11. M. Fourmeau, T. Børvik, A. Benallal, O. Hopperstad, International Journal of Plasticity **48**, 34 (2013)
12. M. Kristoffersen, F. Casadei, T. Børvik, M. Langseth, O. Hopperstad, International Journal of Impact Engineering **71**, 73 (2014)
13. Y. Chen, A. Clausen, O. Hopperstad, M. Langseth, International Journal of Impact Engineering **38**, 824 (2011)
14. M. Kristoffersen, F. Casadei, T. Børvik, M. Langseth, G. Solomos, O. Hopperstad, XII International Conference on Computational Plasticity, Barcelona, Spain (2013)
15. *NS-EN 1991-1-7: Actions on structures - Accidental actions*, Standard Norge (2008)
16. J. Rice, D. Tracey, Journal of Mechanics and Physics of Solids **17**, 201 (1969)
17. V. Tvergaard, A. Needleman, Acta Metallurgica **32**, 157 (1984)
18. R. Tian, S. Chan, S. Tang, A. Kopacz, J.S. Wang, H.J. Jou, L. Siad, L.E. Lindgren, G. Olson, W. Liu, Journal of Mechanics and Physics of Solids **58**, 1681 (2010)
19. P. Mohseni, Ph.D. thesis, Norwegian University of Science and Technology (2012)
20. E. Smith, International Journal of Fracture Mechanics **4**, 131 (1968)
21. T. Anderson, *Fracture mechanics - Fundamentals and applications*, 3rd edn. (Taylor and Francis Group, 2005), ISBN 0-8493-1656-1
22. A. Sabih, J. Nemes, Journal of Materials Processing Technology **209**, 4292 (2009)